

On Catalysis

Edited by

Wladimir Reschetilowski

&

Wolfgang Hönle

VWB – Verlag für Wissenschaft und Bildung
2010

Printed with the support of the
WILHELM OSTWALD-SOCIETY
and
ASSOCIATION OF FRIENDS AND SUPPORTERS OF THE
SAXONIAN ACADEMY OF SCIENCES IN LEIPZIG

The Editors

Prof. Dr. Wladimir Reschetilowski
Technische Universität Dresden
01062 Dresden
Germany

Dr. Wolfgang Hönle
Adolf-Kolping-Str. 26
76275 Ettlingen
Germany

Bibliographic information published by the Deutsche Nationalbibliothek

The Deutsche Nationalbibliothek lists this publication in
in the Deutsche Nationalbibliografie;
detailed bibliographic data are available
in the Internet at <http://dnb.d-nb.de>

ISBN 978-3-86135-232-7

Publisher

VWB – Verlag für Wissenschaft und Bildung, Amand Aglaster
P.O.Box 11 03 68 • 10833 Berlin • Germany
phone: +49-30-251 04 15 • fax: +49-30-251 11 36
e-mail: info@vwb-verlag.com
www.vwb-verlag.com

Copyright

© VWB – Verlag für Wissenschaft und Bildung, 2010

The editors and publisher make no representations, express or implied,
with regard to the accuracy of the information contained in this book
and cannot accept any legal responsibility or liability for any errors or
omissions that may be made.

CONTENTS

Editorial	I
Begleitwort	III
On Catalysis Nobel Lecture by <i>Wilhelm Ostwald</i> on December 12, 1909	1
Climate Protection by an Alternative Use of Methane – The Carbon Moratorium <i>Gerhard Kreysa</i>	17
On Catalysis, Organic Synthesis and Green Chemistry <i>Roger A. Sheldon</i>	32
Catalysis in and with Carbon Dioxide – Current Trends and Recent Examples <i>Martina Peters, Jens Langanke and Walter Leitner</i>	53
Photocatalysis: Perspectives in Fine, Environmental and Green Chemistry <i>Jean-Marie Herrmann</i>	80
Nanochannel Materials for Artificial Photosynthesis <i>Gion Calzaferri and André Devaux</i>	103
Advanced Material Research for Fuel Cells <i>Christian Wieser, Stephan Fell and Josefin Meusinger</i>	127
Acidic Catalysis by Zeolites and the Active Site Concept <i>Joachim Sauer</i>	136
Catalytic Ring Opening in Aromatic Hydrocarbons <i>Jens Weitkamp</i>	162
Olefinpolymerization by Metallocene Catalysis <i>Walter Kaminsky and Gerrit A. Luinstra</i>	186
Supported Ionic Liquid Phase (SILP) Catalysis in Gas Phase Reactions – a Practical Approach to Bridge the Gap between Traditional Homogeneous and Traditional Heterogeneous Catalysis <i>Marco Haumann and Peter Wasserscheid</i>	215
Spatial Heterogeneities within an Individual Catalyst Particle during Reaction as Revealed by In-Situ Micro-Spectroscopy <i>Marianne H.F. Kox and Bert M. Weckhuysen</i>	240
Author Biographies	261

Acidic Catalysis by Zeolites and the Active Site Concept

Joachim Sauer

Institut für Chemie, Humboldt-Universität zu Berlin, Unter den Linden 6, D-10117 Berlin, Germany

Abstract

The interplay of the Brønsted site properties and the framework structure in determining the catalytic function of zeolites as catalysts in hydrocarbon synthesis and hydrocarbon transformation reactions is described from the point of view of quantum chemical modelling. The deprotonation energy is used as parameter for characterising the acid strength of isolated Brønsted sites in different crystallographic positions of a given zeolite, in different framework structures, and in the same framework with different composition (silica vs. aluminium phosphate, faujasites with different Si/Al ratios). The heat of ammonia adsorption as reactivity descriptor is compared with the deprotonation energy. The proton affinity of the substrate is decisive for whether or not it forms a stable protonated species in H-zeolites. It is shown that molecules (or molecular clusters) get protonated if their proton affinity is about that of ammonia (854 kJ/mol) or larger. For the protonation of polar molecules like H₂O or CH₃OH this implies a strong effect of the number of adsorbed molecules per active site (loading) for the protonation state. Stable carbenium ions are formed from aromatic hydrocarbons or cyclic alkenes. The *tert*-butyl carbenium ion is a meta-stable species (minimum on the potential energy surface), but will be converted into isobutene within 85 ms. The importance of adsorption for the observed activation energies is stressed. The heat of adsorption of alkanes increases linearly with the carbon number and decreases with increasing pore size. A Brønsted site makes a constant contribution compared to an all-silica zeolite. The consequences for reliable quantum chemical predictions of apparent energy barriers are discussed and progress in computational methodology is described.

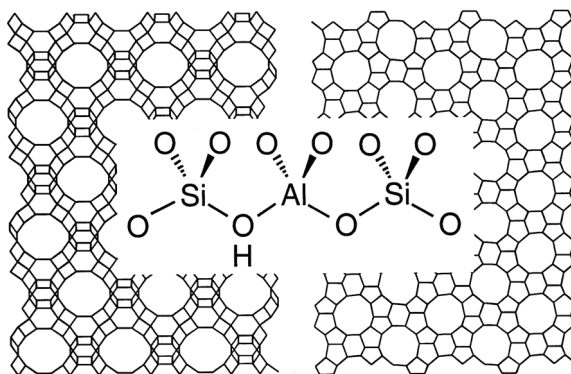
1 Introduction

Acidic catalysis is an important subclass common to homogeneous, enzymatic and heterogeneous catalysis. Among the solid acids used in industrial processes, acidic zeolites¹ are most important because they combine their acid function with selectivity arising from their microporous crystal structure. The gasoline we burn in our car has seen at least one zeolite catalyst on its way through the refinery, and many chemical products, from bulk polymers to fine chemicals, are built up from hydrocarbons in crude oil or natural gas with the help of zeolite catalysts. A prominent example is the conversion of methanol to hydrocarbons, which was first discovered and commercialized by Mobil Oil in 1986 over H-ZSM-5 catalysts.²

Later, Haldor Topsøe developed the Topsøe integrated gasoline synthesis (TIGAS) process,³ Lurgi the methanol to propene (MTP) process,⁴ and Norsk Hydro/UOP the methanol to olefins (MTO) process based on the SAPO-34 catalyst.⁵

However, zeolites are also of outstanding interest from a fundamental point of view. With their well-defined crystalline structure they are a perfect example of the *active site concept*.

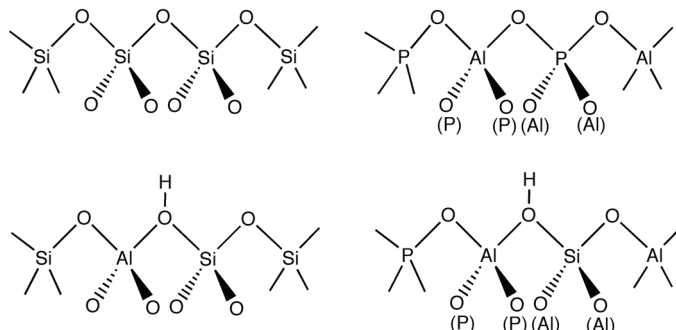
The large variety of zeolite structures⁶ can be described as microporous aluminosilicate polymorphs, $(M^+)_{m}[\text{SiO}_2]_{n-m}[\text{AlO}_2^-]_m$, made of corner-sharing TO_4 tetrahedra ($T=\text{Si}, \text{Al}$). The negative framework charge, defined by the Al content, is compensated by protons or metal cations which are at the origin of the catalytic activity of zeolites. The position of Al in the lattice defines the position of the active site. The proton forms of zeolites, H-zeolites, are strong solid acids.¹ Their Brønsted sites have the proton attached to one of the O atoms of the AlO_4 tetrahedron thus forming bridging hydroxyl groups, Si-O(H)-Al at corner-sharing O atoms connecting the AlO_4 tetrahedron with a neighbouring SiO_4 tetrahedron as illustrated below for two different frameworks:



High silica zeolites are particularly interesting catalysts, because they contain bridging hydroxyl groups as *perfectly isolated active sites*. Two convincing experiments that use the n-hexane cracking activity as test reaction show this. For H-MFI catalysts (trivial name H-ZSM-5), the activity changes linearly with the Si/Al ratio between 100000 and 20.⁷ Two catalysts, H-FAU and H-MFI, with the same Si/Al ratio of 26 have nearly the same specific activities, 11.4 and 8.5 mmol/(g min), respectively.⁸

If we consider an AlPO_4 -framework instead of an SiO_2 -framework and then replace P by Si/H (see formula below), we obtain a catalyst with the same Si-O(H)-Al active site, but with a different framework composition.

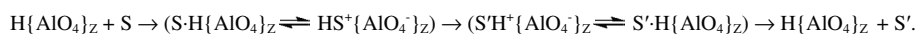
Strictly, these catalysts are not zeolites (this name is reserved for aluminosilicates), but aluminiumphosphates (AIPOs) or silicon-aluminium-phosphates (SAPOs). It is indeed possible to synthesize acidic high-silica (H-SSZ-13)⁹ and SAPO catalysts (H-SAPO-34)¹⁰ with the same chabasite (CHA) framework structure.¹¹



In the following we will use quantum chemical simulations to describe active site properties and their variation with the structure and composition of the framework (Si/Al ratio, silica vs. aluminium phosphate). We will look at the ability to protonate substrate molecules and the interplay of active site properties and framework structure for the activity and reactivity in hydrocarbon conversion and synthesis reactions.

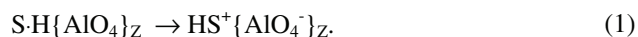
2 Proton Transfer to Substrate Molecules within Zeolite Cavities

In acidic catalysis, it is assumed that the substrate molecule S is activated for further conversion into S' by proton transfer from the zeolite,

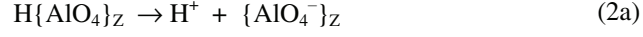


Inspired by the chemistry in superacidic media, it has been speculated that zeolites may be superacids, able to protonate even saturated hydrocarbon molecules to yield carbonium ions as a first step of catalytic cracking. Later, doubts have been raised if carbenium ions obtained by protonation of unsaturated hydrocarbons are stable intermediates that can be found experimentally or if they are merely transition structures in the catalytic reaction cycle. From the theoretical point of view the question is: Are they minima (stable structures) or saddle points (transition structures) on the potential energy surface? However, even if they are minima, they may be separated by very small barriers from products or their neutral complex counterparts and, hence, transient species that are difficult to detect experimentally.

Whether or not the neutral adsorption complex or the ion-pair structure is more stable depends on the energy of the proton transfer reaction, ΔE_{PT} ,



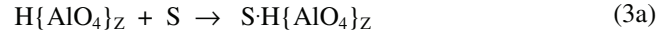
It can be decomposed into the deprotonation energy, $E_{DP}(Z)$ of the zeolite,



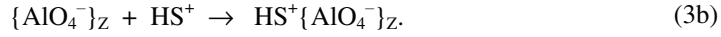
the proton affinity of the substrate, $-E_{PA}(S)$,



the binding energy of the substrate on the neutral zeolite surface, $-E_{NC}(S)$,



and the binding energy of its protonated counterpart on the deprotonated zeolite surfaces, $E_{IP}(SH^+)$,



Hence,

$$\Delta E_{PT} = E_{DP}(Z) - E_{PA}(S) - E_{NC}(S) + E_{IP}(SH^+). \quad (4)$$

If we ignore all interactions between substrate and zeolite, the *proton affinity* is the characteristic parameter that describes the relative reactivity of different substrates with regard to protonation by a given zeolite, whereas the *deprotonation energy* describes the relative ability of different zeolites to protonate a given substrate. Note that the deprotonation energy of the zeolite, $H\{AlO_4\}_Z$, is up to the sign equal to the proton affinity of the deprotonated zeolite, $\{AlO_4^-\}_Z$.

Instead of ignoring the interaction with the substrate, we can include them for a "model" substrate and use the energy of ammonia desorption to characterize the acid strength of zeolites.



The ammonia adsorption energy defined by the reverse of eq. 5 is composed of the energy of the (hypothetical) desorption of NH_4^+ from the active site $\{AlO_4^-\}_Z$ and a subsequent proton transfer from NH_4^+ to the $\{AlO_4^-\}_Z$ site,

$$E_{ad}(NH_3) = E_{DP}(Z) - E_{PA}(NH_3) + E_{IP}(NH_4^+). \quad (6)$$

3 Isolated Brønsted Sites in Different Framework Structures and Compositions

In the faujasite (FAU) and chabazite (CHA) lattices, there is only one crystallographically distinct T site and, hence, only one possibility to create an isolated Al site. However, there are four possible O sites to which the proton can be attached creating four different bridging hydroxyl groups (Figure 1).

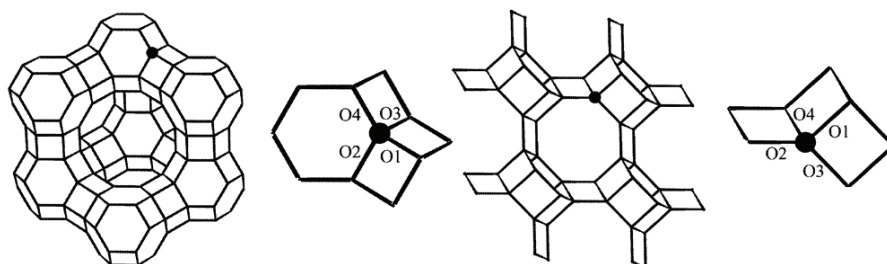


Figure 1 Fragments of faujasite (left) and chabazite lattices (right) with numbering of oxygen sites. For simplicity, oxygen atoms are not shown

Table 1 OH stretching frequencies for Brønsted sites in different zeolites^a

	H-FAU O1H	H-MFI O7H	H-CHA O1H	H-FER O7H	H-CHA O3H	H-FAU O3H
Obsd. ^a	3623	3614, 3610	3603	3598	3579	3550
Hybrid	3626	3608	3606 ^b	3609 ^c	3588 ^b	3563
QM:MM ^a						

^a ref. ¹² except otherwise noted, B3LYP/T(O)DZP, scaled by 0.9716;

^b Average for different cluster models, variation 8 cm⁻¹;

^c B3LYP/TZVP, scaled by 0.9614, ref. ¹⁵.

The predicted¹² energetic order of proton locations was O1 < O3 < O4 < O2 for H-FAU and O1 < O3 < O2 < O4 for H-CHA. This is in agreement with the assignment of the two bands in the OH stretching region of the infrared spectra to O1 and O3 sites for both H-FAU¹³ and H-CHA¹⁴ (note the different numbering in ref. ¹⁴). The calculated OH frequencies reproduce the experimental sequence of wavenumbers OH1-FAU > O1H-CHA > O3H-CHA > O3H-FAU (Table 1) which shows that the computational method applied is able to correctly model the effect of the framework structure on the Brønsted site properties.

The variation of the calculated energies of deprotonation in Table 2 across different catalysts H-ZSM-5, H-MOR, H-SSZ13, and H-FER is small, within 15 kJ/mol only. The framework composition is more important, as demonstrated for the Si/Al ratio in Section 4 (Figure 2). For Brønsted sites in aluminium phosphate frameworks (H-SAPO-34), the calculated deprotonation energies are higher by 30 - 40 kJ/mol, i.e., the acidity is predicted to be lower in agreement with experimental observations.

4 Brønsted Sites and the Al Distribution in Faujasite

The concentration of Al in the framework (and its distribution) are additional features by which different acidic zeolites can vary, however within limits. The Löwenstein rule forbids Al-O-Al links between AlO_4^- tetrahedra and the minimum Si/Al ratio is 1. Moreover, for low Si/Al ratios, not all charge-compensating cations can be protons and typically there are Na^+ ions left.

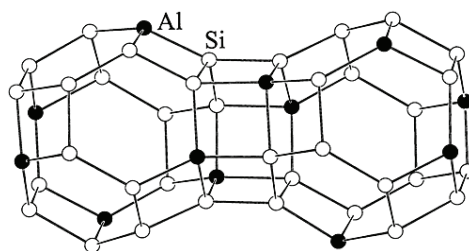
Table 2 Energies of deprotonation (kJ/mol) calculated by different methods for Brønsted sites of different zeolite catalysts^a

Zeolite		QM-Pot HF ^b	QM-Pot B3LYP ^c	Plane wave BLYP ^d
HSAPO-34	CHA		1261	1276
H-ZSM-5	MFI	1235		
H-MOR	MOR	1230		
H-SSZ-13	CHA	1225	1231	1235
H-Y ^c	FAU	1220 ^e	1224 ^c	
H-FER(O7)	FER		1218 ^f	
H-FAU	FAU	1206	1198	

^a To eliminate the effect of different systematic errors in different quantum chemical models, a constant is added for each of the models. It is obtained by calibration calculations for the related molecules methanol and silanol, for which very accurate deprotonation energies are known; ^b Corrected by -46 kJ/mol,¹⁶ data from refs. ^{17,18}; ^c The systematic error is zero and no correction is necessary, refs. ^{19,20}; ^d Corrected by 38 kJ/mol, ref. ²⁰; ^e ref. ²¹; ^f ref. ¹⁵

For more than one Al in the lattice, electrostatic arguments predict that Al atoms assume the largest possible distance for a given Si/Al ratio²² which is known as Dempsey's rule. For two Al substitutions in the primitive faujasite cell (24 T atoms), explicit lattice energy minimizations, confirmed by quantum chemical cluster calculations,²³ showed strong preference for Al-O-Si-O-Al pairs in four-membered rings when one proton was added to an oxygen atom of each AlO₄ tetrahedron. This finding is not a peculiarity of the faujasite lattice, but was also found for other frameworks featuring double six-ring secondary building units (offretite, zeolite L, erionite, chabasite, gmelinite).²³

The heterogeneity of the Brønsted acid strength resulting from the Al distribution in faujasites has been examined by calculating deprotonation energies for two types of materials: High-silica faujasite with isolated or paired Al sites (1 or 2 Al per 48 T sites) and Y-type materials with Si/Al ratios of 3 and 2.43. For the latter, we adopt the distribution pattern of refs.,^{24,25} the only one found²⁴⁻²⁷ that was compatible with the measured NMR intensities and obeyed Lowenstein's rule:



Even for an isolated Brønsted site with only one crystallographically distinct Al site in the FAU lattice, the preference for O1 and O3 occupation and the assignment of the respective OH groups to high frequency (HF) and low frequency (LF) infrared bands is well-established and reproduced by hybrid QM:MM calculations.^{12,17,21} For the 2.43 and 3.0 Si/Al ratios, O1:O2:O3:O4 proton occupation patterns of 8:2:4:0 and 7:2:3:0, respectively, have been adopted which are close to the ratios inferred from powder neutron diffraction experiments.

Figure 2 shows the calculated OH stretching frequencies as a function of the calculated deprotonation energies.²¹ The most important observation is that the former are primarily determined by the local structure (O1 or O3) while the latter primarily depend on the number of Al atoms in next-nearest-neighbor position. The overall Si/Al ratio seems to affect the acid strengths of a particular site only indirectly, the lower the Si/Al ratio the higher the probability that next nearest Al neighbours exist.

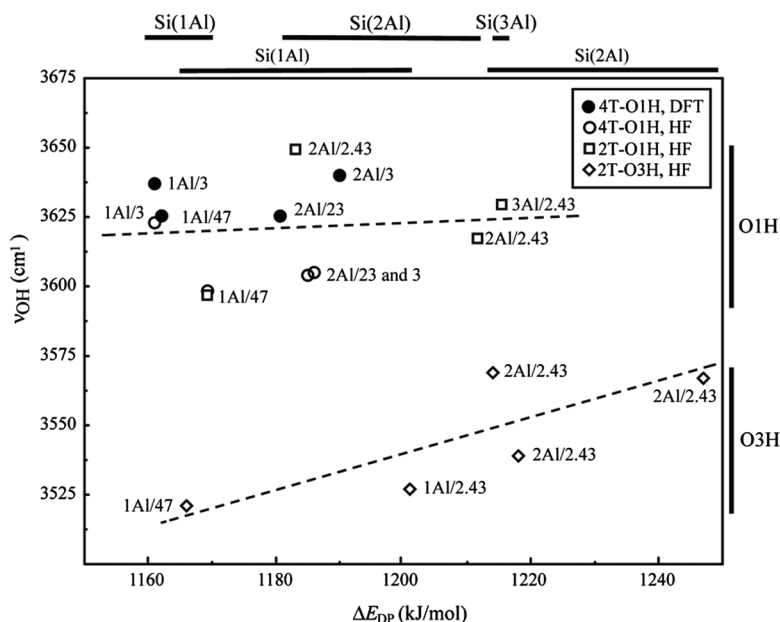


Figure 2 OH stretching frequencies and energies of deprotonation of bridging hydroxyl groups in H-faujasites as a function of the Al content.²¹ "2Al/3" means that there is a second Al in next-nearest-neighbor position and that the Si/Al ratio in the framework is 3. The bars "O1" and "O3" on the right side indicate the range of data for the two types of O positions

5 Ammonia, Methanol and Water Molecules in H-zeolites

A common experimental means of characterizing the acidity of zeolites is the use of probe molecules. IR spectra leave no doubt that ammonium ions are formed upon adsorption of ammonia in zeolites, the OH band characteristic for bridging Si-O(H)-Al sites disappears and NH_4^+ bending bands appear.²⁸ The energy of ammonia desorption, eq. 5, is used to characterize the acid strength of zeolites. Usually it is obtained from temperature programmed desorption, but true equilibrium values require calorimetric measurements.

Quantum chemical studies by a hybrid QM:MM method¹⁸ (Table 3) confirm the formation of NH_4^+ ions on interaction of ammonia with Brønsted sites in zeolites. The proton transfer energies are around -30 kJ/mol. No calculation that includes the full periodic structure of the zeolite has found a local minimum for a neutral adsorption complex. Energies of deprotonation indicate that H-FAU releases its proton most easily, yet the heat of NH_3 adsorption (eq. 6) is largest for H-MOR. The reason is that binding of NH_4^+ onto the zeolite surface, $E_{IP}(\text{NH}_4^+)$, is less favorable in the large pore zeolite FAU (12-rings of $\text{SiO}_{4/2}$ units) than in the smaller pores of

the other zeolites (CHA, MOR, MFI) with 8- and 10-rings. These calculations assumed that the Brønsted site is created at the crystallographic T position at which Al is most stable, but differences for Al in different crystallographic T positions are small, usually a few kJ/mol. For H-MOR DFT calculations have shown that the location of the Brønsted site can have a large effect on the heat of NH₃ adsorption. Values of -126 to -128 kJ/mol (close to the results of ref. ¹⁸) are found for Al in sites 1 and 2, but for Al in site 3 a much larger value of -152 kJ/mol is obtained.²⁹ The reason is that in this case NH₄⁺ can bind via four N-H...O bonds to the zeolite framework. It coordinates with three N-H bonds to oxygen atoms of an 8-ring and points with one N-H bond into the so-called side pocket of the MOR framework. Only for H-FAU the calculated heats of adsorption are in the range of reported calorimetric results. For H-CHA, H-MFI and H-MOR they are much lower. Even if adsorption in the side pocket is assumed for H-MOR, the predicted heat of adsorption would be about 20 kJ/mol too low.

For adsorption of a series of structurally related molecules in the same zeolite, eq. 6 implies a correlation between the measured heat of adsorption and the proton affinity of that molecule, provided that the ion-pair binding energy, $E_{IP}(MH^+)$, is constant or changes with the proton affinity. For adsorption of ammonia and methyl-substituted amines on H-MFI and H-MOR, such a correlation has indeed been reported³¹ with deviations for trimethylamine and n-butylamine. Both can be explained by deviations from the prevailing adsorbate structure. Protonated trimethylamine can form only one hydrogen bond with the zeolite framework, and for n-butylamine the van der Waals (dispersion) interaction of the butyl chain contributes to the binding on the zeolite surface in addition to the two hydrogen bonds.

In conclusion, due to its high proton affinity (854 kJ/mol) ammonia gets always protonated in any H-zeolite. The proton affinities of methanol (754 kJ/mol) and water (691 kJ/mol) are significantly lower than that of ammonia and whether or not these molecules are protonated in H-zeolites has created lively debates in the literature.

For H-zeolites with high Si/Al ratios early DFT calculations showed that methanol is not protonated in hypothetical H-sodalite,³² but for H-chabasite an ion-pair structure of protonated methanol within an 8-ring was found by energy minimization.³³ This caused speculations³⁴ that "a direct correlation between zeolite structure and chemical activation of the adsorbate" might exist which³³ could not be confirmed. Subsequent Car Parrinello Molecular Dynamics (CPMD) simulations for CHA³⁵ revealed that the ion-pair complex is a stationary point on the potential energy surface that is reached during MD only 4 times within 2.5 ps for very short time. The global minimum structure is the neutral complex which is 18 kJ/mol more stable, see ref.³⁶ for a confirmation. Later, neutral adsorption structures for zeolites with large unit cells, TON,³⁷ FER(10-ring channel)^{36,37} and MFI³⁶⁻³⁸ were found.

Table 3 Proton transfer energy, ΔE_{PT} , deprotonation energy, E_{DP} , hypothetical binding energy of NH_4^+ on the deprotonated zeolite surfaces, $E_{IP}(SH^+)$, and energy of ammonia adsorption, $E_{ad}(NH_3)$, (kJ/mol) for Brønsted sites in different zeolite frameworks¹⁸

Zeolite ^a	H-FAU (47)	H-CHA (11)	H-MOR (47)	H-MFI (95)
ΔE_{PT}	-32	-35	-34	-29
E_{DP}	1206	1225	1230	1235
$E_{IP}(NH_4^+)$	-457 (2)	-476 (3)	-484 (2)	-480 (2)
$E_{ads}(NH_3)$ ^b	-109	-109	-116	-106
$E_{ads}(NH_3)$, MP2 ^c	-127	-128	-133	-123
$H_{ads}(NH_3)$ ^d	-113	-114	-119	-109
$E_{ads}(NH_3)$, DFT		-123; -133 ^e	-126... -128 ^f	
$H_{ads}(NH_3)$, obsd. ^g	-115...-130	-155	-160	-145; -150

^a In parentheses: Si/Al ratio assumed in the calculations. ^b Hartree-Fock results. ^c Final electronic energy including electron correlation (MP2). ^d Calculated heat of adsorption, includes estimates for zero-point vibrational energy and thermal corrections (298 K). ^e B3LYP, ref.³⁰. ^f PW91, Al in T1 and T2-sites, bidentate, for Al in T3 -site, tetradentate adsorption with stronger binding, -152, is obtained, ref.²⁹ ^g See ref.¹⁸ for the original references to microcalorimetry, for MOR see also ref.²⁹

The calculated (PBE functional) heat of adsorption in MFI, 86 kJ/mol, gets very close to the experimental value, 115 ± 5 kJ/mol,³⁹ after adding a semiempirical dispersion term (115 kJ/mol for PBE+dispersion).³⁸

The measured ¹H NMR chemical shift for methanol in H-ZSM-5 (9.4 ppm) was much larger than for liquid methanol (4.7 ppm) and in the same range as the shift observed for methanol in the FSO₃H-SbF₅-SO₂ superacid (9.4 ppm).⁴⁰ This was taken as a hint that methoxonium species might have formed in H-zeolites, although the authors did not exclude alternative interpretations. There was no information about the chemical shift of the methoxonium protons when interacting via hydrogen bonds with the zeolite surface. However, quantum calculations could provide such information. Figure 3 shows the ¹H NMR chemical shifts calculated for methanol and the methoxonium ion, both hydrogen-bonded to the zeolite surface.⁴¹ The methoxonium protons undergo a huge shift from 6.2 down to 17.4 ppm when interacting with the zeolite surface in the ion-pair complex, which is much larger than the observed value of 9.4 ppm.^{40,42} In the neutral complex, the Brønsted site proton also undergoes a similarly large shift due to the strong hydrogen bond from

2.9 to 14.6 ppm, while the methanol proton extends a weaker hydrogen bond to the zeolite framework and its NMR signal shifts less, from 0.0 to 7.0 ppm. An average shift of 10.8 ppm due to a fast exchange of the zeolite and methanol protons was predicted⁴¹ which is close to the observed value.

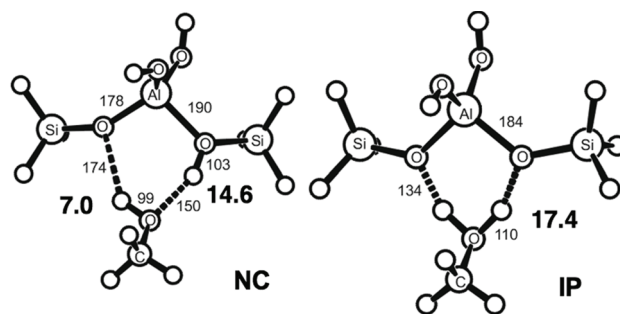


Figure 3 ¹H NMR chemical shifts (ppm) for methanol (NC - neutral adsorption complex) and methoxonium (IP - ion pair complex) interacting with the zeolite surface

Support for a neutral hydrogen-bonded adsorption complex comes also from a measurement of the distance between the methanol and the zeolite protons in H-MOR by wide line ¹H NMR at 4 K, 193-200 pm,⁴³ which is in good agreement with the calculated equilibrium distances for H-CHA (188 pm),³⁵ TON (189; 192 pm) and H-FER (190 pm),³⁷ while the H-H distance calculated for methoxonium adsorbed in CHA is much smaller, 158 pm.³⁵ The agreement of spectroscopic parameters with predictions for neutral adsorption complexes, of course, does not exclude the possibility that surface methoxonium ions would exist as a minority species in equilibrium. That the methoxonium ion is not a (meta-stable) local minimum structure but a transition structure is concluded from quantum calculations mentioned above.

For the adsorption of two methanol molecules per bridging hydroxyl groups (2:1 loading) studies on all zeolites, SOD⁴⁴, CHA^{36,45}, FER³⁶ agree that a protonated methanol dimer is formed. The obvious reason is the high PA of the methanol dimer (887 kJ/mol) compared to the monomer (757 kJ/mol) that exceeds even the PA of ammonia (858 kJ/mol).

High-silica zeolites are known to be hydrophobic and it is also known since long that the water uptake at a given pressure is a function of the aluminium content, i.e. of the number of Brønsted sites.⁴⁶⁻⁴⁸ At standard temperature and modest water pressure (e.g., p/p₀ = 0.6), typically four water molecules per Al are adsorbed suggesting formation of a H₅O₄⁺ species. Quantum chemical calculations on cluster models showed that the neutral adsorption complex is a minimum on the PES (stable structure), while the hydroxonium ion corresponds to a transition structure for proton exchange.^{49,50} Infrared spectra obtained for a loading level of a single water

molecule per Brønsted site have been interpreted as either due to a neutral hydrogen bonded molecule or due to formation of a hydroxonium ion. The calculations for ion-pair complex could not explain the characteristic pair of bands in the hydrogen-bond region (2877 and 2463 cm^{-1} , see Fig. 3) whereas those for the neutral adsorption complex could.⁴⁹ The crucial experiment was the isotope substitution (^{18}O) of water⁵¹ which showed no effect on the pair of bands at 2877 and 2463 cm^{-1} and thus clearly supported their assignment to vibrations of the zeolitic Brønsted site. Due to hydrogen bonding with the adsorbed H_2O molecule, the zeolitic OH stretching is strongly red-shifted and Fermi resonance with the overtone of the in-plane SiOH bending creates an Evans window at the overtone position, see ref.⁵² for a recent model calculation.

Figure 4 shows the observed spectrum⁵¹ and the assignment based on MP2 frequency calculations.⁴⁹ The predicted position of the zeolitic OH stretch band (red-shifted and broadened due to hydrogen bonding) falls close to the predicted position of the overtone of the in-plane SiOH bending. The bands at 3698 and 3558 are assigned to OH stretch of the free and hydrogen bonded protons of the adsorbed H_2O molecule, and the bands at 1629 and 1353 to the HOH and SiOH bendings. Additional support came from inelastic neutron scattering results which showed agreement with the neutral complex only.⁵³

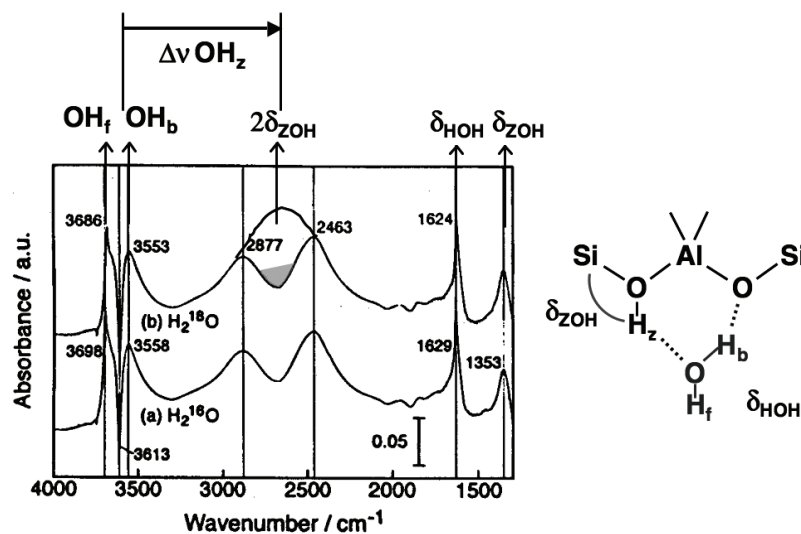


Figure 4 IR spectrum of H_2^{16}O and H_2^{18}O adsorbed on H-ZSM-5 (adapted from ref.⁵¹). Shown is the assignment based on MP2 calculations for models of the neutral adsorption complex⁴⁹

Thus it came as a surprise when a neutron diffraction study on H-SAPO-34 seemed to provide evidence for a protonated water molecule.⁵⁴ A comment to the

original paper in the same issue pointed out that a loading higher than one H₂O molecule per Brønsted site may be responsible for the observed protonation of water in the experimental study.⁵⁵ Indeed, both cluster studies mentioned^{49,50} and a DFT study applying periodic boundary conditions⁴⁴ found that a second water molecule per Brønsted site yields H₃O₂⁺ attached to the surface as an energy minimum structure. Subsequently, two periodic DFT simulations of the H₂O/H-SAPO-34 system^{56,57} analyzed the role of an increasing number of water molecules in detail. To match the composition of the experimental sample as closely as possible, a double cell of the CHA structure was chosen with one Brønsted site in one cell and two in the other cell.⁵⁶ When a simulation with 4 H₂O molecules per 3 Brønsted sites was made, one water molecule moved from the cage with one OH group into the cage with two OH groups and the three molecules together had a high enough proton affinity to form a H₇O₃⁺ cluster stabilized by H-bonds with the wall of the SAPO material.⁵⁶

This perfectly fits our picture that the proton transfer depends on the proton affinity of the adsorbed molecule: the proton affinity of the water trimer (853 kJ/mol, Table 5) is about that of ammonia (858 kJ/mol).

If the CHA framework is not aluminium phosphate, as in H-SAPO-34, but silica, as in H-SSZ-13, the ion-pair structure is found more stable for a loading of two to four molecules per site (Table 4),⁵⁸ but the detailed answer depends on the specific density functional applied in the calculations. Table 4 shows that the Becke-Lee-Yang-Parr (BLYP) functional yields smaller adsorption energies and gives more weight to neutral adsorption complexes than the Perdew-Burke-Ernzerhofer (PBE) functionals. For a loading of two molecules per site, another interesting result is obtained, if a double cell is used for the simulation. A heterogeneous distribution of one molecule per site in the first cell and three molecules per site in the second cell is energetically slightly more stable than (BLYP) or equally stable as (PBE) the homogeneous distribution. This may have implications for the interpretation of experiments. For example, an IR spectrum obtained for an average loading of 2:1 may be composed of spectra for 1:1 (neutral hydrogen bonded) and 3:1 complexes (ion-pair structures).

The most accurate value for the binding energy of the first water molecule to H-CHA, 78 kJ/mol, has been obtained by a hybrid MP2:PBE method including extrapolation to the complete basis set limit.⁵⁹ Comparison with the DFT results of Table 4 indicates that PBE (76 kJ/mol) yields more reliable energies than BLYP (62 kJ/mol). The predicted heat of adsorption at 298 K, 73 kJ/mol, can be compared with heats of adsorption of 80±10 kJ/mol obtained from isotherms for H-ZSM-5⁴⁸ and with about 80 kJ/mol obtained by calorimetric measurements for both H-ZSM-5 and H-BEA.⁶⁰ For loadings of two to four water molecules, DFT adsorption energies are rather constant and about 15 kJ/mol lower than for a loading of one molecule per site (Table 4). This is in agreement with the observed decrease of the heat of adsorption for H-ZSM-5 from 80±10 (n=1) to 63±10 (n=2-4)⁴⁸ and from about 80 (n=1) to about 60 (n=2-4).⁶⁰

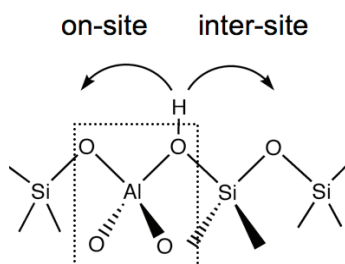
Table 4 Binding energies per water molecule (kJ/mol) for different loadings in H-CHA^a

Global loading (molecules per acid site)	Functional Complex	BLYP		PBE	
		NC	IP	NC	IP
1:1	1:1	62 (53)	–	76 (71)	–
	0:1/2:1	48	–	61	–
1.5:1	1:1/2:1	53	–	67	–
	0:1/3:1	–	44	–	57
2:1	2:1	46 (39)	45 (38)	–	61 (56)
	2:1/2:1	48	47	–	63
	1:1/3:1	49 (40)	–	63 (55)	–
	0:1/4:1	–	39	–	53
3:1	3:1	–	45 (37)	–	59 (51)
4:1	4:1	–	45 (35)	–	60 (51)

^a ref.⁵⁸; the values in parenthesis include zero point energy corrections.

5 Proton Mobility in H-zeolites

For an unloaded H-zeolite, there are four oxygen sites around Al to which the proton can be attached. In most zeolites proton affinities are different for these oxygen sites and some will be preferred. For zeolite FAU, two OH frequencies and two ¹H NMR shift signals can be experimentally resolved, which are unequivocally assigned to O1H and O3H sites. For higher temperatures, on-site proton jumps between the different oxygen atoms of an AlO₄⁻ site may be possible.



Translational proton motion through the zeolite lattice appears to be much less likely because the proton has to leave the {AlO₄}_Z site and move to {SiO₄}_Z sites

that have a lower proton affinity. DFT calculations for a typical Brønsted site in H-MFI (Si/Al=95)⁶¹ yield an inter-site barrier of 127 kJ/mol for leaving the $\{\text{AlO}_4\}_Z$ site.⁶¹ The highest barrier for proton transfer from $\{\text{AlO}_4\}_Z$ site to $\{\text{AlO}_4\}_Z$ site along a path of $\{\text{SiO}_4\}_Z$ sites is 202 kJ/mol.

Quantum chemical calculations for the six different on-site jump paths between the oxygen atoms of the AlO_4^- site have been made for three different framework structures, CHA, FAU and MFI.¹² For jumps from the most stable proton sites, transition state theory yields rates of the order of $1 - 100 \text{ s}^{-1}$ at room temperature and of the order of $10^5 - 10^6 \text{ s}^{-1}$ at 500 K.¹²

The presence of residual amounts of small molecules like water or ammonia left over from the preparation process may significantly reduce barriers for proton motion by a vehicle mechanism. Already for a coverage of Brønsted sites with water molecules at the ppm level the kinetics is dominated by the very much faster H_2O assisted jumps.⁶² The hybrid MP2:DFT study for the $\text{H}_2\text{O} - \text{Brønsted}$ site complex that includes the full periodic zeolite at the DFT level yields barriers (including zero-point vibrational contributions) of 65 and 20 kJ/mol for $\text{O}^1 - \text{O}^2$ jumps in dry and water loaded H-CHA (1:1), respectively. At room temperature, this increases the jump rate by eight orders of magnitude from 40 to 30×10^8 per second. The nanosecond time scale at which H_2O assisted proton jumps can hence be expected is not accessible by CPMD simulations which typically are run for picoseconds. This explains that during CPMD simulations for the 1:1 $\text{H}_2\text{O}/\text{H-CHA}$ system mentioned above, proton jumps from one framework oxygen to another one via a hydroxonium transition structure have not been observed, whereas proton transfer between the water trimer and the zeolitic Brønsted site occurred on the picosecond time scale.

6 Stability of Carbenium Ions in Zeolites

Nicholas and Haw concluded that stable carbenium ions in zeolites are observed by NMR if the parent compound (from which the carbenium ion is obtained by protonation) has a proton affinity of 875 kJ/mol or larger.⁶³ Simulations by quantum methods discussed in section 4 showed that this statement is more general and that proton transfer from a H-zeolite to a molecule or molecular cluster occurs if its proton affinity is about that of ammonia (854 kJ/mol) or larger.⁵⁶ In the light of eq. 4 this means that proton transfer occurs, $\Delta E_{\text{PT}} \leq 0$, if $E_{\text{DP}}(\text{Z}) - E_{\text{NC}}(\text{S}) + E_{\text{IP}}(\text{SH}^+)$ is smaller than 854 kJ/mol. Table 5 shows proton affinities and indicates in which cases and by which method protonated species have been detected.

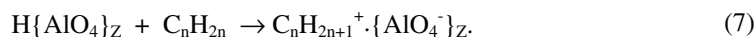
Table 5 Proton affinities, $H_{PA}(298)$ of molecules and clusters (kJ/mol) and observation of protonated species in zeolites

Parent compound ^a	Obsd. ^a	MP4 ^b	Other ^c	Evidence
water	691		694	
benzene	750	746		
propene	751	742		
cyclopentene	766	759		
methanol	754		757	
toluene	784			
isobutene	802	805		
water dimer			806	
m-xylene	811			
3-methylphenyl-(2,4-dimethylphenyl)-methane		821 ^d		DFT ^d
water trimer			853	DFT ^f
<i>ammonia</i>	854		858	IR ^g
hexamethylbenzene	861			UV-vis ^e
1-methylindene		878		NMR ^b
methanol dimer			887	DFT ^h
water tetramer			895	DFT ^f
1,3-dimethylcyclopentadiene		902		NMR ^b
pyridine	929	917		IR, NMR
1,5,6,6-tetramethyl-3-methylene-cyclohexa-1,4-diene		951		NMR ^b
3,6-dimethylene-cyclohexa-1,4-diene		1031 ^d		DFT ^d

^a ref. ⁶⁴; ^b ref. ⁶³, except otherwise noted; ^c MP2/DZP, unpublished data; ^d ref. ⁶⁵;

^e ref. ⁶⁶; ^f ref. ^{56,58}; ^g ref. ²⁸; ^h ref. ⁴⁵

Carbenium ions can be formed by proton transfer from the Brønsted site to an unsaturated hydrocarbon which requires a negative proton transfer energy, eq. 4.

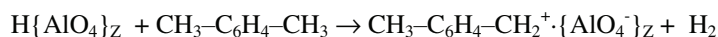


Alternatively, carbenium ions can be formed by hydride abstraction from a saturated hydrocarbon,



In the latter case, the lifetime of the carbenium ion formed will be limited by transferring a proton back to the zeolite, thus completing the dehydrogenation of the hydrocarbon.

Hydride abstraction from xylene is assumed to be the initial step of its disproportionation into toluene and trimethylbenzene.⁶⁵



The parent compound of the carbenium ion formed, $\text{CH}_2=\text{C}_6\text{H}_4=\text{CH}_2$, has such a high proton affinity (1031 kJ/mol, Table 5) that proton transfer back to the zeolite does not occur at all. For this species, experimental evidence is not yet available, but Table 5 lists three examples of cyclic alkenyl carbenium ions with lower proton affinity that live long enough in zeolites to be detected by NMR.⁶³

The *tert*-butyl cation observed in superacidic media is of fundamental interest as the smallest stable non-cyclic carbenium ion. Even if the proton affinity of isobutane (802 kJ/mol, Table 5) does not make it very likely that it will exist in zeolites, two quantum chemical studies^{67,68} reached the conclusion that the *tert*-butyl cation is a local minimum on the potential energy surface and, hence, a possible intermediate. There are additional deactivation channels for carbenium ions. They can attach via C-O bonds to the zeolite framework and form alkoxides as shown in Fig. 5 for isobutene.

Figure 5 shows the reaction energy profile with the *tert*-butyl carbenium ion (**1**) 60 kJ/mol less stable than adsorbed isobutene (**2**) as well as 24 and 51 kJ/mol less stable than *tert*-butoxide (**3**) and isobutoxide (**4**), respectively. Nevertheless, **1** may be formed as an intermediate, for example in the skeletal isomerization of butenes⁷¹ or by reacting *tert*-butyl halides with alkaline ion exchanged zeolites⁷². Its lifetime will then depend on the barriers separating it from isobutene and the alkoxides. The barrier separating **1** from the most stable adsorbed isobutene **2** is 17.5 kJ/mol yielding a half life $\tau_{1/2} = \ln 2/k = 59 \mu\text{s}$ (transition state theory). For detection by NMR⁷³ this is probably not long enough, but the time-scale of UV/Vis spectroscopy⁷⁴ should in principle allow for the detection of this carbenium ion once it has formed, e.g. from *tert*-butyl halides.

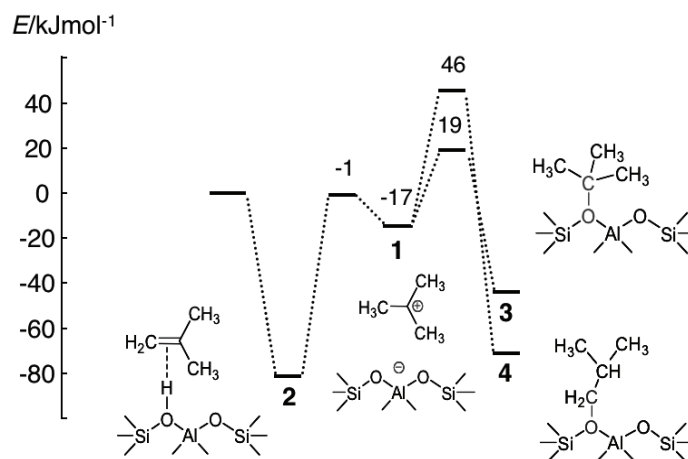


Figure 5 Potential energy profile for the isobutene/H-FER system calculated with the hybrid MP2:DFT method^{69,70}

The latter results have been obtained with a multi-level hybrid method that yields results of near chemical accuracy.⁶⁹ By combining MP2 calculations for the reaction site with DFT calculations for a large system under periodic boundary conditions, it yields MP2 quality results for the full periodic structure. In addition, it includes also higher order corrections for the electron correlation energy at the CCSD(T) level, evaluated for small models. This way, two problems of currently used density functionals are solved: the inability to properly account for dispersion interactions yielding too small adsorption energies and the self-interaction correction error leading to too low barriers and too stable polar structures (protonated molecules). For the present case pure DFT (left hand side of Fig. 5) yields a barrier of only 5.2 kJ/mol, a half life that is two orders of magnitude shorter (0.42 μ s) and only a small fraction of the adsorption energy of isobutene (17 instead of 77 kJ/mol).

7 Interplay of Adsorption and Reaction Steps

Figure 6 shows the energy profile for a reaction on the surface of a solid catalyst. It applies to the internal surfaces of zeolites, but also to flat surfaces, for example of oxides. To be converted at the active site, the substrate has first to bind onto the surface, forming a catalyst-substrate complex, C-S. If the conditions are such that an adsorption equilibrium is established, the rate of product formation depends on the rate constant for the *intrinsic* reaction step, k_{intr} , and on the surface concentration of the substrate. The latter is given by the adsorption equilibrium constant, K_{ads} , and the gas pressure. The rate of the product formation, r_p , is obtained from the gas pressure, p_S , and the apparent rate constant,

$$r = k_{\text{app}} \cdot p_G \quad \text{with} \quad k_{\text{app}} = K_{\text{ads}} \cdot k_{\text{intr}}$$

Hence, the reaction is controlled by the *apparent* energy barrier, which is the sum of the *intrinsic* energy barrier and the heat of adsorption,

$$E_{\text{app}} = \Delta H_{\text{ads}} + E_{\text{intr}}$$

A striking example is the strong decrease of the measured (Arrhenius) barriers for the alkane cracking with increasing carbon number N_C , see E_{app} in Table 6.⁷⁵ When the heat of adsorption is independently measured, the intrinsic barrier can be calculated and it becomes obvious that it varies within a narrow range only, whereas the heat of adsorption increases linearly with the carbon number.

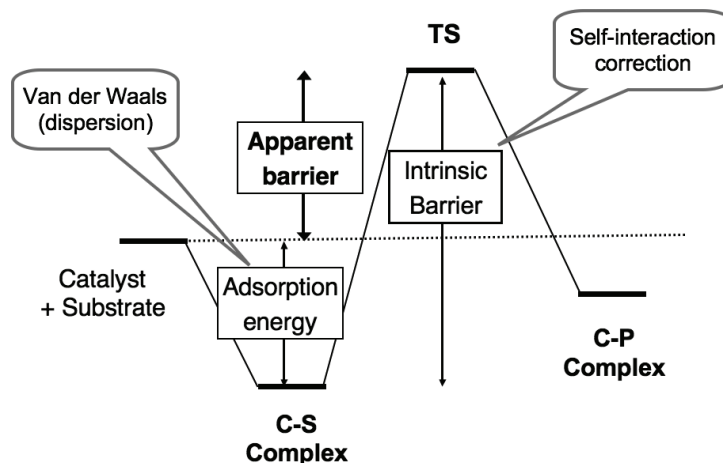


Figure 6 Energy profile for a surface reaction showing the adsorption (C-S – catalyst-substrate complex) and reaction steps (TS – transition structure; C-P – catalyst-product complex)

Lercher *et al.* have measured the heats of adsorption of alkanes in different zeolites,⁷⁶⁻⁷⁸ and found a linear dependency on the carbon number,

$$-\Delta H_{\text{ads}}(N_C) = a + b \cdot N_C. \quad (9)$$

Table 7 shows the increments b and the predicted values for methane, $N_C = 1$. The uncertainty of the measured heats is at least ± 2 kJ/mol and this is also the uncertainty of the parameters in the Table 7. The results for the all-silica structures MFI and FAU are similar to the results found by careful temperature programmed desorption experiments for the MgO(100) surface. The increments b decrease with the "pore size" considering a flat surface as the limiting case of an infinitely large pore:

MFI > FAU > MgO(100).

They show a similar behaviour for the proton forms of the zeolites,

H-MFI > H-MOR > H-MFI.

The predicted values for CH₄ are in the range 9.6 to 13.7 kJ/mol for the oxides free of Brønsted sites, whereas values between 21.4 and 29.2 kJ/mol are obtained for the proton forms, resulting in increments of around 12 kJ/mol for the presence of the Brønsted site (12.4 and 11.8 kJ/mol for H-MFI – MFI and for H-FAU – FAU, respectively).

Table 6 Apparent and intrinsic energy barriers for alkane cracking in H-MFI as well as enthalpies of adsorption as function of the carbon number, N_C (kJ/mol)^a

N_C	E_{app}	E_{intr}	ΔH_{ads}
4	142	205	-63
6	125	205	-80
8	92	197	-105
9	84	197	-113
10	67	192	-125

^a ref. ⁷⁵, 811K, low pressure and conversion.

Table 7 Predicted heat of adsorption for methane, $-\Delta H_{ads}(CH_4)$, and increment per CH₂ unit for higher alkanes, b, eq. 9 (kJ/mol)

	Ring size	$-\Delta H_{ads}(CH_4)=a+b$	b
MgO(100) ^a	∞	12.6	7.2
FAU ^b	12	9.6	8.1
MFI ^b	10	13.7	11.7
H-FAU ^c	12	21.4	5.1
H-MOR ^c	8, 12	29.2	6.7
H-MFI ^c	10	26.1	11.2

^a ref. ⁷⁹; ^b ref. ⁷⁸; ^c ref. ⁷⁷

The linear increase points to van der Waals (dispersion) interactions as the origin of the binding onto the oxide surfaces. The electrostatic and polarization effects arising from the Brønsted sites make a constant contribution to alkanes of increasing size.

The data presented demonstrate that different frameworks with different pore sizes affect observed reaction rates primarily by different adsorption strengths, whereas the intrinsic activity of Brønsted sites varies little with the different framework structures.

8 Energy Barriers for Alkylation Reactions

For the synthesis of hydrocarbons from methanol, the hydrocarbon pool mechanism has been proposed⁸⁰ which assumes that light alkenes are formed via repeated methylation and dealkylation reactions of aromatic reaction centers.^{81,82} Understanding such complex mechanisms of hydrocarbon synthesis and conversion reactions requires information for individual steps. While conditions of experiments can seldom be chosen such that elementary steps can be resolved, quantum chemistry together with transition state theory can be employed and the rate constants obtained for the individual steps can then be used in a microkinetic model of the whole reaction network.

Experimental rate constants are available for the methylation of small alkenes with methanol,⁸³ which are apparent with respect to the alkene as illustrated in Figure 6. They served as a test set for different quantum chemical calculations. Even if periodic boundary conditions are applied, the large size of zeolite unit cells and the large number of atoms in a unit cell represent a computational challenge. Density functional theory was very helpful over the last decade in suggesting mechanisms,⁸⁴ but the energy barriers obtained are affected by two types of errors already mentioned in section 6 and illustrated in Figure 6: the inability to properly account for dispersion interactions yielding too small adsorption energies and the self-interaction correction error leading to too low barriers. The partial compensation of these two errors may sometimes lead to DFT barriers that are in surprisingly good agreement with measured barriers, but also to serious disagreement for closely related cases.

The methylation of ethane, propene and butene is a striking example for this.³⁸ Figure 7 shows that the pure DFT barrier (labelled "periodic PBE") is 15 kJ/mol larger than the experimental barrier, but the deviation increases for propene and butene to 35 and 56 kJ/mol, respectively. The reason is that the underestimation of the intrinsic barrier is about the same for all three alkenes, whereas the missing dispersion contribution increases with the number of carbon atoms (see section 7). If we add a semiempirical dispersion term to the DFT energy (labelled "periodic PBE-D" in Fig. 7) the barriers are systematically too low (14-19 kJ/mol) as typical of this type of functionals. The *hybrid MP2:DFT* method of Tuma and Sauer⁶⁹ mentioned above which takes both effects into account yields reaction barriers with near chemical accuracy (deviations between 0 and 13 kJ/mol).

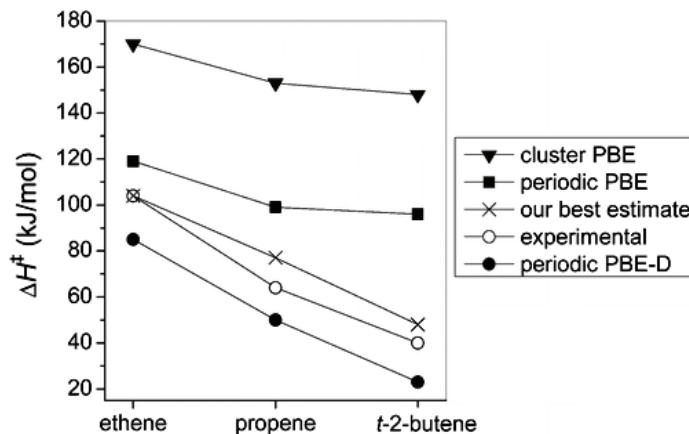


Figure 7 Apparent enthalpy barrier for the methylation of alkenes in H-MFI obtained with different methods³⁸

The same method has been applied to the alkylation of benzene by ethane over H-MFI.⁸⁵ Both for the one-step and a two step mechanism (formation of ethoxide as intermediate) are considered. Intrinsic rate coefficients calculated by means of transition state theory are converted to apparent quantities by means of the multicomponent adsorption equilibrium. The simulated turnover frequencies are close to experimental data.

Whereas predictions of energy barriers with near chemical accuracy have already been reported for well-characterized enzymes,⁸⁶ this is now also possible for individual steps of hydrocarbon synthesis and conversion reactions in zeolites. With this, substantial progress has been made toward the simulation of complex reaction networks in zeolites such as the hydrocarbon pool mechanism.

Acknowledgements

This work has been supported by the Cluster of Excellence "Unifying Concepts in Catalysis" in Berlin, by the Priority Programme 1155 and by the Norddeutscher Verbund für Hoch- und Höchstleistungsrechner (HLRN, computer time).

10 References

- [1] A. Corma, *Chem. Rev.* **1995**, 95, 559-614.
- [2] J. Cobb in *New Zealand Synfuel: The Story of the World's First Natural Gas to Gasoline Plant*, Cobb/Horwood Publications, Auckland, New Zealand, **1995**, p. 1.
- [3] J. Topp-Jorgensen, *Stud. Surf. Sci. Catal.* **1988**, 36, 293.

- [4] H. Koempel, W. Liebner, *Stud. Surf. Sci. Catal.* **2007**, *167*, 261.
- [5] J. Q. Chen, A. Bozzano, B. Glover, T. Fuglerud, S. Kvisle, *Catal. Today* **2005**, *106*, 103.
- [6] C. Baerlocher, L. B. McCusker in *Database of zeolite structures*, www.iza-structure.org/databases, **2007**.
- [7] W. O. Haag, R. M. Lago, P. B. Weisz, *Nature (London)* **1984**, *309*, 589-591.
- [8] J. R. Sohn, S. J. DeCanio, P. O. Fritz, J. H. Lunsford, *J. Phys. Chem.* **1986**, *90*, 4847-4851.
- [9] S. I. Zones, *J. Chem. Soc. Chem. Commun.* **1995**, 2253.
- [10] L. J. Smith, L. Marchese, A. K. Cheetham, J. M. Thomas, *Catal. Lett.* **1996**, *41*, 13.
- [11] W. M. Meier, D. H. Olson in *Atlas of Zeolite Structure Types*, Butterworths-Heinemann, London, **1992**.
- [12] M. Sierka, J. Sauer, *J. Phys. Chem. B* **2001**, *105*, 1603-1613.
- [13] M. W. Anderson, J. Klinowski, *ZEOLITES* **1986**, *6*, 455-466.
- [14] L. J. Smith, A. Davidson, A. K. Cheetham, *Catal. Lett.* **1997**, *49*, 143-146.
- [15] V. Nieminen, M. Sierka, D. Y. Murzin, J. Sauer, *J. Catal.* **2005**, *231*, 393-404.
- [16] J. Sauer in *Modelling of Structure and Reactivity in Zeolites* (Ed. C. R. A. Catlow), Academic Press, London, **1992**, pp. 183-216.
- [17] U. Eichler, M. Brändle, J. Sauer, *J. Phys. Chem. B* **1997**, *101*, 10035-10050.
- [18] M. Brändle, J. Sauer, *J. Am. Chem. Soc.* **1998**, *120*, 1556-1570.
- [19] M. Sierka, J. Sauer, *Faraday Discuss.* **1997**, *106*, 41-62.
- [20] J. Sauer, K.-P. Schröder, V. Termath, *Coll. Czech. Chem. Commun.* **1998**, *63*, 1394-1408.
- [21] M. Sierka, U. Eichler, J. Datka, J. Sauer, *J. Phys. Chem. B* **1998**, *102*, 6397-6404.
- [22] E. Dempsey, G. H. Köhl, D. H. Olson, *J. Phys. Chem.* **1969**, *73*, 387-390.
- [23] K.-P. Schröder, J. Sauer, *J. Phys. Chem.* **1993**, *97*, 6579-6581.
- [24] G. Engelhardt, U. Lohse, E. Lippmaa, M. Tarmak, M. Magi, *Z. Anorg. Allg. Chem.* **1981**, *482*, 49-64.
- [25] J. Klinowski, S. Ramdas, J. M. Thomas, C. A. Fyfe, J. S. Hartman, *J. Chem. Soc. Faraday Trans II* **1982**, *78*, 1025-1050.
- [26] S. Ramdas, J. M. Thomas, J. Klinowski, C. A. Fyfe, J. S. Hartman, *Nature* **1981**, *292*, 228-230.
- [27] G. Engelhardt, E. Lippmaa, M. Magi, *J. Chem. Soc. Chem. Commun.* **1981**, 712-713.
- [28] Y. Yin, A. L. Blumenfeld, V. Gruver, J. J. Fripiat, *J. Phys. Chem. B* **1997**, *101*, 1824-1830.
- [29] T. Bucko, J. Hafner, L. Benco, *J. Chem. Phys.* **2004**, *120*, 10263-10277.
- [30] X. Solans-Monfort, M. Sodupe, V. Branchadell, J. Sauer, R. Orlando, P. Ugliengo, *J. Phys. Chem. B* **2005**, *109*, 3539-3545.
- [31] C. Lee, D. J. Parrillo, R. J. Gorte, W. E. Farneth, *J. Am. Chem. Soc.* **1996**, *118*, 3262-3268.

- [32] E. Nusterer, P. E. Blöchl, K. Schwarz, *Angew. Chem., Int. Ed.* **1996**, *35*, 175-177, *Angew. Chem.* **1996**, *108*, 187-189.
- [33] R. Shah, J. D. Gale, M. C. Payne, *J. Phys. Chem.* **1996**, *100*, 11688-11697.
- [34] R. Shah, M. C. Payne, M.-H. Lee, J. D. Gale, *Science* **1996**, *271*, 1395-1397.
- [35] F. Haase, J. Sauer, J. Hutter, *Chem. Phys. Lett.* **1997**, *266*, 397-402.
- [36] I. Stich, J. D. Gale, K. Terakura, M. C. Payne, *J. Am. Chem. Soc.* **1999**, *121*, 3292-3302.
- [37] F. Haase, J. Sauer, *Micropor. Mesopor. Mat.* **2000**, *35-36*, 379-385.
- [38] S. Svelle, C. Tuma, X. Rozanska, T. Kerber, J. Sauer, *J. Am. Chem. Soc.* **2009**, *131*, 816-825.
- [39] C. C. Lee, R. J. Gorte, W. E. Farneth, *J. Phys. Chem. B* **1997**, *101*, 3811-3817.
- [40] M. W. Anderson, P. J. Barrie, J. Klinowski, *J. Phys. Chem.* **1991**, *95*, 235-239.
- [41] F. Haase, J. Sauer, *J. Am. Chem. Soc.* **1995**, *117*, 3780-3789.
- [42] M. Hunger, T. Horvath, *J. Am. Chem. Soc.* **1996**, *118*, 12302-12308.
- [43] L. Heeribout, C. Doremieux-Morin, L. Kubelkova, R. Vincent, J. Fraissard, *Catal. Lett.* **1997**, *43*, 143-147.
- [44] E. Nusterer, P. E. Blöchl, K. Schwarz, *Chem. Phys. Lett.* **1996**, *253*, 448-455.
- [45] J. Sauer, M. Sierka, F. Haase in *Transition State Modeling for Catalysis*, ACS Symposium Series 721 (Eds.: D. G. Truhlar, K. Morokuma), American Chemical Society, Washington, **1999**, pp. 358-367.
- [46] N. Y. Chen, *J. Phys. Chem.* **1976**, *80*, 60.
- [47] D. H. Olson, W. O. Haag, R. M. Lago, *J. Catal.* **1980**, *60*, 390.
- [48] D. H. Olson, W. O. Haag, W. S. Borghard, *Micropor. Mesopor. Mat.* **2000**, *35-36*, 435-446.
- [49] M. Krossner, J. Sauer, *J. Phys. Chem.* **1996**, *100*, 6199-6211.
- [50] S. A. Zygmunt, L. A. Curtiss, L. E. Iton, M. K. Erhardt, *J. Phys. Chem.* **1996**, *100*, 6663-6671.
- [51] F. Wakabayashi, J. N. Kondo, K. Domen, C. Hirose, *J. Phys. Chem.* **1996**, *100*, 1442-1444.
- [52] V. V. Mihaleva, R. A. van Santen, A. P. J. Jansen, *J. Chem. Phys.* **2004**, *120*, 9212-9221.
- [53] H. Jobic, A. Tuel, M. Krossner, J. Sauer, *J. Phys. Chem.* **1996**, *100*, 19545-19550.
- [54] L. J. Smith, A. K. Cheetham, R. E. Morris, L. Marchese, J. M. Thomas, P. A. Wright, J. Chen, *Science* **1996**, *271*, 799-802.
- [55] J. Sauer, *Science* **1996**, *271*, 774-775.
- [56] V. Termath, F. Haase, J. Sauer, J. Hutter, M. Parrinello, *J. Am. Chem. Soc.* **1998**, *120*, 8512-8516.
- [57] Y. Jeanvoine, J. G. Angyan, G. Kresse, J. Hafner, *J. Phys. Chem. B* **1998**, *102*, 7307-7310.

- [58] M. V. Vener, X. Rozanska, J. Sauer, *Phys. Chem. Chem. Phys.* **2008**, *11*, 1702-1712.
- [59] C. Tuma, J. Sauer, *Chem. Phys. Lett.* **2004**, *387*, 388-394.
- [60] V. Bolis, S. Bordiga, C. Lamberti, A. Zecchina, A. Carati, F. Rivetti, G. Spanò, G. Petrini, *Micropor. Mesopor. Mat.* **1999**, *30*, 67-76.
- [61] M. E. Franke, M. Sierka, U. Simon, J. Sauer, *Phys. Chem. Chem. Phys.* **2002**, *4*, 5207-5216.
- [62] J. A. Ryder, A. K. Chakraborty, A. T. Bell, *J. Phys. Chem. B* **2000**, *104*, 6998-7011.
- [63] J. B. Nicholas, J. F. Haw, *J. Am. Chem. Soc.* **1998**, *120*, 11804-11805.
- [64] E. P. Hunter, S. G. Lias in *NIST Chemistry WebBook, NIST Standard Reference Database Number 69* (Eds.: P. J. Linstrom, W. G. Mallard), National Institute of Standards and Technology, Gaithersburg MD, 20899, **2005**.
- [65] L. A. Clark, M. Sierka, J. Sauer, *J. Am. Chem. Soc.* **2003**, *125*, 2136-2141.
- [66] M. Bjorgen, F. Bonino, S. Kolboe, K.-P. Lillerud, A. Zecchina, S. Bordiga, *J. Am. Chem. Soc.* **2003**, *125*, 15863-15868.
- [67] C. Tuma, J. Sauer, *Angew. Chem., Int. Ed.* **2005**, *44*, 4769-4771, *Angew. Chem.* **2005**, *117*, 4847-4849.
- [68] M. Boronat, P. M. Viruela, A. Corma, *J. Am. Chem. Soc.* **2004**, *126*, 3300-3309.
- [69] C. Tuma, J. Sauer, *Phys. Chem. Chem. Phys.* **2006**, *8*, 3955-3965.
- [70] C. Tuma, T. Kerber, J. Sauer, *Angew. Chem., Int. Ed.* **2010**; in press.
- [71] A. Boronat, A. Corma, *Appl. Catal. A* **2008**, *336*, 2-10.
- [72] R. J. Correa, C. J. A. Mota, *Phys. Chem. Chem. Phys.* **2002**, *4*, 4268-4274.
- [73] N. D. Lazo, B. R. Richardson, P. D. Schettler, J. L. White, E. J. Munson, J. F. Haw, *J. Phys. Chem.* **1991**, *95*, 9420-9425.
- [74] H. Ishikawa, E. Yoda, J. N. Kondo, F. Wakabayashi, K. Domen, *J. Phys. Chem. B* **1999**, *103*, 5681-5686.
- [75] W. O. Haag in *Zeolites and Related Microporous Materials: State of the Art 1994. Proceedings of the 10th International Zeolite Association Meeting*, Stud. Surf. Sci. and Catal., Vol. 84 (Eds.: J. Weitkamp, H. G. Karge, H. Pfeifer, W. Hölderich), Elsevier, Amsterdam, **1994**, pp. 1375-1394.
- [76] F. Eder, J. Lercher, *J. Phys. Chem. B* **1997**, *101*, 1273-1278.
- [77] F. Eder, M. Stockenhuber, J. A. Lercher, *J. Phys. Chem. B* **1997**, *101*, 5414-5419.
- [78] F. Eder, J. Lercher, *ZEOLITES* **1997**, *18*, 75-81.
- [79] S. L. Tait, Z. Dohnalek, C. T. Campbell, B. D. Kay, *J. Chem. Phys.* **2005**, *122*, 164708-164701 - 164708-164713.
- [80] I. M. Dahl, S. Kolboe, *J. Catal.* **1994**, *149*, 458.
- [81] J. F. Haw, W. Song, D. M. Marcus, J. B. Nicholas, *Acc. Chem. Res.* **2003**, *36*, 317-326.
- [82] U. Olsbye, M. Bjorgen, S. Svelle, K. P. Lillerud, S. Kolboe, *Catal. Today* **2005**, *106*, 108.

- [83] S. Svelle, P. O. Ronning, U. Olsbye, S. Kolboe, *J. Catal.* **2005**, *234*, 385-400.
- [84] J. Hafner, L. Benco, T. Bucko, *Top. Catal.* **2006**, *37*, 41-54.
- [85] N. Hansen, T. Kerber, J. Sauer, A. T. Bell, F. J. Keil, submitted.
- [86] F. Claeysens, J. N. Harvey, F. R. Manby, R. A. Mata, A. J. Mulholland, K. E. Ranaghan, M. Schütz, S. Thiel, W. Thiel, H. J. Werner, *Angew. Chem., Int. Ed.* **2006**, *45*, 6856-6859.